Nano Research 2018, 11(5): 2705–2714
https://doi.org/10.1007/s12274-017-1900-0
Research Article

ISSN 1998-0124
CN 11-5974/O4

Soft thermal nanoimprint lithography using a nanocomposite mold

Viraj Bhingardive, Liran Menahem, and Mark Schvartzman (✉)

Department of Materials Engineering, Isle Katz Institute of Nanoscale Science and Technology, Ben-Gurion University of the Negev, P.O. Box 653, Beer-Sheva 8410501, Israel

Received: 6 September 2017
Revised: 15 October 2017
Accepted: 25 October 2017

KEYWORDS
soft lithography,
nanoimprint lithography,
polydimethylsiloxane (PDMS),
non-planar substrates

ABSTRACT

Soft nanoimprint lithography has been limited to ultraviolet (UV) curable resists. Here, we introduce a novel approach for soft thermal nanoimprinting. This unprecedented combination of the terms "soft" and "thermal" for nanoimprinting became possible thanks to an innovative nanocomposite mold consisting of a flexible polydimethylsiloxane (PDMS) substrate with chemically attached rigid relief features. We used soft thermal nanoimprinting to produce high-resolution nanopatterns with a sub-100 nm feature size. Furthermore, we demonstrate the applicability of our nanoimprint approach for the nanofabrication of thermally imprinted nanopatterns on non-planar surfaces such as lenses. Our new nanofabrication strategy paves the way to numerous applications that require the direct fabrication of functional nanostructures on unconventional substrates.

1 Introduction

Soft nanoimprinting is a versatile, high-throughput, and cost-effective nanolithography method in which a nanoscale pattern is mechanically transferred onto a resist by an elastomeric mold. Today, elastomeric molds are commonly produced from polydimethylsiloxane (PDMS) [1, 2]. As a mold material, PDMS has numerous advantages over its rigid counterparts such as Si, quartz, or Ni [3]. First, PDMS has a relatively low surface energy of ~ 20 $mN \cdot m^{-1}$ [4], and its molds therefore do not require any anti-sticking agents, which are necessary for rigid molds [5]. In addition, PDMS molds are much less sensitive to surface contaminants than rigid molds, so the nanopatterns produced by PDMS molds are practically free of defects. In addition, nanoimprint with soft molds does not require high pressure; it can be performed by gentle pressing with the thumb [6]. Finally, flexible PDMS molds can be applied to non-planar surfaces. This last advantage is particularly important for the production of functional nanostructures on curved or flexible substrates [7, 8].

In addition to its numerous benefits, soft nanoimprint has several drawbacks, the most notable of which is the inability of PDMS molds to produce nanopatterns with a sub-100 nm resolution. This limitation stems from the low modulus of PDMS, whose relief features deform and collapse during imprinting [9]. Notably, such a limitation does not exist for nanoimprinting

Address correspondence to marksc@bgu.ac.il

with rigid molds with features that can be down-sized to several nanometers [10]. Improving the mechanical properties of PDMS was proposed by Schmid et al. who formulated hard PDMS and used it as a material for high-performance stamps for microcontact printing [11]. Inspired by this innovation, Odom et al. designed a hybrid PDMS mold with a hard PDMS-based imaging layer and used it for nanoimprinting with a sub-100 nm resolution [12]. However, some limitations remain with respect to the application of such molds, such as the fact that they generate cracks in the hard imaging layer. Later, Li et al. reported a soft mold composed of a PDMS substrate and imaging layer made of a photocurable polymer, demonstrating sub-15 nm resolution and the ability to imprint the surface of an optical fiber [13]. Yet, it should be noted that such a mold can form a conformal contact with a fiber by bending around its cylindrical surface (Fig. 1(a)). On the other hand, imprinting a surface with a more complex curvature, such as a lens or saddle, would require in-plane stretching of the mold (Fig. 1(b)), which is impossible for a hybrid mold with a continuous, stiff imaging layer.

In addition to resolution, nanoimprint molds must be also examined in terms of their compatibility with different imprint resists. In this sense, rigid molds, which can be used with both ultraviolet (UV) curable and thermal resists, are highly advantageous over

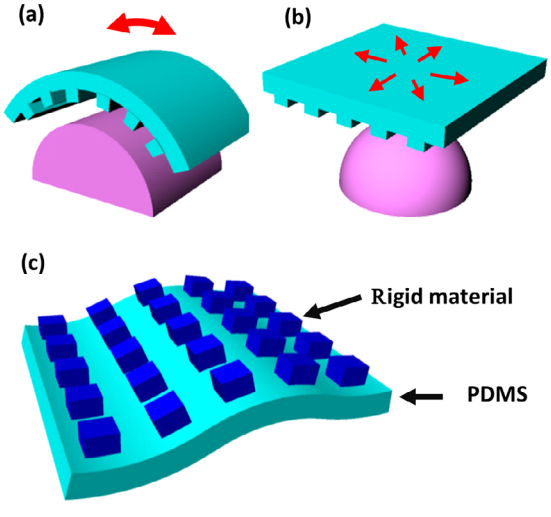

Figure 1 Schematic representation of (a) soft mold imprinting on fiber and (b) soft mold imprinting on a lens. (c) Nanocomposite mold made of a soft flexible PDMS substrate with chemically attached rigid relief nanofeatures.

soft molds that are limited to UV curable resists. The incompatibility of soft nanoimprint molds with thermal resist stems from the fact that a typical thermal resist, such as, commonly used PMMA, has an elastic modulus of 1–3 MPa while heated to its imprint temperature of 160–200 ˚C [14]. This modulus is similar to that of PDMS [15]. Thus, while PDMS relief features are pressed against a viscous resist, they do not completely penetrate it but rather deform and collapse. This feature deformation leads to a significant distortion of the imprinted pattern. The incompatibility of soft nanoimprinting with thermal resists has precluded many of its important applications such as direct embossing of curved thermoplastic substrates. We hypothesize that thermal nanoimprinting of curved substrates is only possible with an elastic mold, which would not deform while pressed against a viscous resist because of its stiff relief features.

Here, we report for the first time the soft nanoimprinting of a thermal resist. To overcome the limitations of soft nanoimprinting, as listed above, and make it compatible with thermal resists, we designed an innovative nanocomposite mold based on an elastic PDMS substrate onto which rigid silica nanofeatures were chemically tethered (Fig. 1(c)). Notably, the rigidity of the features ensured robust pattern transfer into a thermal resist, with a pattern fidelity that is typical for hard nanoimprinting. We produced nanocomposite molds with various nanopatterns comprising relief features with different sizes and shapes. We compared the nanopatterns produced by our nanocomposite molds with those generated by conventional PDMS molds. We found that nanocomposite molds can thermally imprint sub-100 nm features, whereas conventional PDMS molds are incompatible with thermal resists. Furthermore, we used our nanocomposite molds to imprint a thermoplastic film on a lens, which represents the first thermal nanoimprint on a curved substrate.

Rigid nanofeatures cannot be directly fabricated on PDMS substrate because of a few reasons. First, PDMS has very low surface energy and any deposited thin film therefore will poorly adhere to it [16]. Furthermore, such thin films would likely crack due to the surface elasticity, even when well-adhered. Finally, PDMS swells in various organic solvents [17].

Therefore, the fabrication of rigid nanofeatures onto a PDMS substrate requires an "out-of-the-box" approach. Here, we applied a pattern transfer process [18] to fabricate a PDMS mold with nanosized rigid relief features made of cured spin-on-glass material. The schematic fabrication process flow is shown in Fig. 2(a). First, we evaporated a 40-nm thick Au film on a sacrificial silicon substrate. Notably, Au was deposited directly on Si without any adhesion layer. We then applied a film of hydrogen silsesquioxane (HSQ, XR-1541, Dow Corning) and patterned it using electron-beam lithography by exposing it in a Raith E-line system, developing it in TMAH solution (AZ 726, Rohm and Haas) for 2 min, rinsing it in DI water, and drying it. Notably, HSQ is widely used as a spin-on-glass precursor [19]. In addition, it is also a well-known inorganic electron beam resist with the best achievable resolution because its cage-like molecular structure transforms into a cross-linked network upon electron beam radiation [20]. Therefore, HSQ is an ideal material for ultra-small silica nanofeatures directly fabricated by lithography and without any complementary pattern transfer process such as plasma etching. To complete the transformation of the electron-beam-exposed HSQ to nonstoichiometric silicon oxide, we thermally annealed it for 30 min at 330 °C and then ashed it in oxygen plasma (Harrick PDC-32G, 1 min). We then applied a thin film of PMMA (A6, 495K, Microchem GmbH) by spin coating and baked it for 2 min at 180 °C. We used thermal tape (Revapha, Nitto Denko) to peel the entire structure from the Si wafer and stripped the Au film by immersing the tape into a standard iodine-based etchant, potassium iodide (KI), for half a minute, followed by immediate rinsing in DI water and nitrogen drying. To attach the HSQ features to a premade PDMS substrate (Sylgard 184, Dow corning, see the Electronic Supplementary Material (ESM) for details), we first exposed both the thermal tape with the embedded HSQ features and PDMS substrate to oxygen plasma (Harrick PDC-32G, 1 min), which activates their surfaces with hydroxyl groups [21]. Immediately after the plasma exposure, we gently pressed the two surfaces against each other for 1 s using our thumb and baked the sandwiched substrates overnight in an oven at 60 °C. No additional pressure was applied on the substrates during baking. Finally, we detached the thermal tape by briefly heating the sample to 110 °C using a hot plate and removed the PMMA by rinsing it with acetone.

We verified the completion of the transfer of the

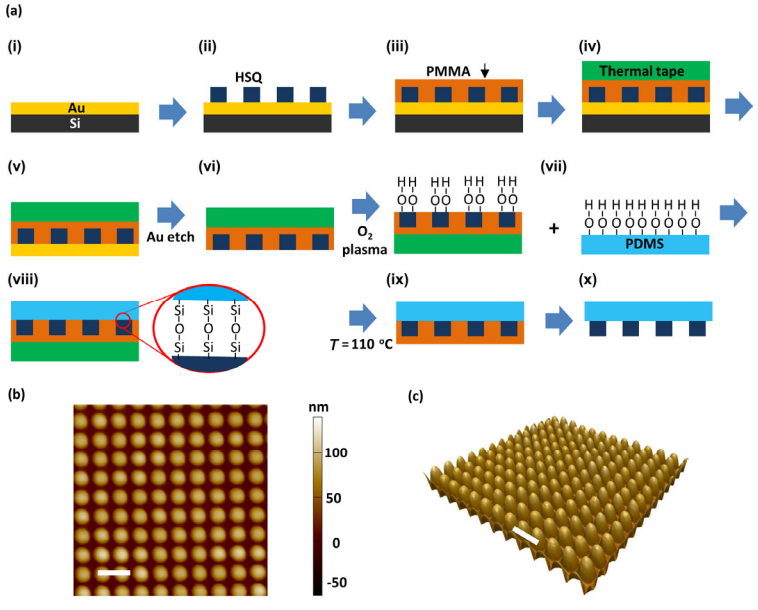

Figure 2 (a) Process flow for the fabrication of a nanocomposite mold: (i) deposition of Au on the sacrificial Si substrate; (ii) HSQ electron-beam lithography and thermal annealing; (iii) deposition of the PMMA film; (iv) application of thermal tape; (v) detachment from silicon; (vi) Au etching; (vii) oxygen plasma treatment of both PDMS and exposed features; (viii) pressing the two surfaces against each other and baking; (ix) detachment of thermal tape by heating the assembly; and (x) stripping PMMA. (b) Top-view AFM image of a nanocomposite mold. (c) 3D top-view AFM image of a nanocomposite mold (the scale bar is 500 nm in both cases).

HSQ features onto the PDMS substrate by scanning the surface of the obtained mold with an atomic force microscope (AFM). Figures 2(b) and 2(c) show representative AFM images of a nanocomposite PDMS mold with HSQ relief features that have been chemically attached to its surface using the described pattern transfer process. We compared the HSQ features before and after the transfer and found that their shape, size, height, and morphology did not change during the transfer (Fig. S1 in the ESM). We found that the produced composite structure is highly robust. For instance, neither high-power sonication for 10 min nor exposure to a temperature higher than 100 °C caused any observable damage of the mold. We believe that this robustness stems from strong and irreversible Si–O–Si covalent bonds formed at the PDMS–HSQ interface [22]. Also, PDMS is known to swell in organic liquids including acetone [17]. Yet, we found that the short exposure of the mold to acetone during the last fabrication step did not lead to any observable morphology change, neither for the PDMS surface nor for the HSQ features. Furthermore, any possible swelling of PDMS can, in principle, be prevented by using a water-soluble polymer such as polyvinyl alcohol (PVA) instead of PMMA.

To ensure that the demolding of the HSQ relief features from the resist will be easy and robust, we treated the fabricated molds with a mold release agent based on a fluorinated silane monolayer (Nanonex NXT 110). Such fluorinated silanes have been extensively used as mold release agents for Si- and SiO_2-based molds. Furthermore, the same mold release agents were shown to be effective for Si molds with relief features made from electron-beam patterned and thermally cured HSQ [23]. We hypothesize that organic silanes form a self-assembled monolayer on a HSQ surface, as they do on a silica surface, because the composition of cured and plasma-treated HSQ is close to that of silica [24–26]. This hypothesis has been recently confirmed by demonstrating that polyethylene glycol silanes can chemically passivate the surface of cured HSQ [27].

To demonstrate the compatibility of our nanocomposite molds for thermal nanoimprinting, we used polybenzylmethacrylate (PBMA) as a thermal resist. We chose PBMA due to its relatively low glass transition point of 54 °C, which allows thermal nanoimprinting at a temperature below 100 °C [28]. Such a low imprint temperature should prevent any substantial changes in the mechanical properties of PDMS that can be caused by overheating [29, 30]. We diluted PBMA in toluene, spin-coated it on a silicon substrate, and baked it at 100 °C for 2 min. We used a Nanonex XB200 imprinting tool for nanoimprinting. The typical process parameters included a temperature of 90 °C, pressure of 100 psi, and process time of 5 min. For each mold, we applied a PBMA film with a thickness that was slightly higher than the height of the mold features, thereby ensuring robust polymer flow during the imprint and preventing air trapping between the features.

To explore the resolution limits of soft thermal nanoimprinting, we produced nanocomposite PDMS–HSQ molds patterned with arrays of rectangular or circular features of various sizes. To demonstrate the uniqueness of our soft thermal nanoimprint approach, we compared the obtained nanoimprinted patterns to patterns imprinted with regular PDMS molds [31] prepared by casting PDMS onto the electron beam-patterned PMMA film and curing (see Fig. S2 and the description in the ESM for details).

Figure 3 compares the nanoimprinted arrays of circular features with a diameter of 1 μm, produced with a regular PDMS mold and a nanocomposite PDMS–HSQ mold. As shown in the top view AFM image (Fig. 3(c)), the features imprinted with the regular PDMS mold barely replicate the circular shape of the mold features (Fig. S3(a) in the ESM). Furthermore, these imprinted features have a conical shape as seen in the cross-sectional AFM image (Fig. 3(e)), which is most probably due to the deformation of the relief features pressed against the viscous resist. In contrast, similar features imprinted using the composite PDMS–HSQ and observed in both top-view and cross-sectional AFM images (Figs. 3(d) and 3(f)), precisely reproduced the mold geometry (Fig. S3(b) in the ESM).

Notably, few cracks are visible on the surface of PBMA imprinted with the nanocomposite mold (Fig. 3(f)). We speculate that they replicate defects of the mold surface, which could have formed either by

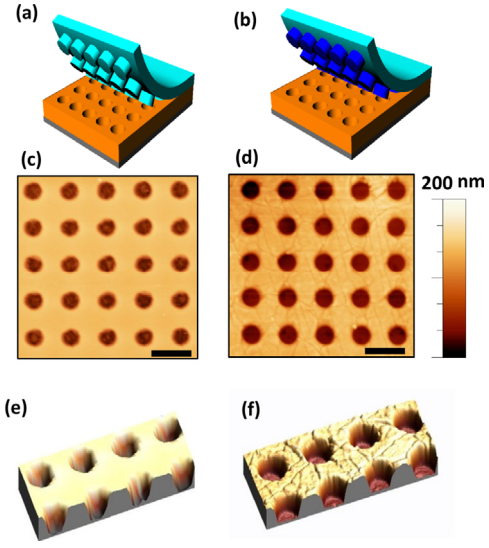

Figure 3 Comparison between a soft PDMS mold and PDMS–HSQ hybrid mold. (a) Schematic showing imprinting with the soft PDMS mold. (b) Schematic showing imprinting with the PDMS–HSQ hybrid mold. (c) AFM image of the substrate after imprinting with the soft PDMS mold. (d) AFM image of the substrate after imprinting with the PDMS–HSQ hybrid mold. (e) and (f) Cross-sectional view of the imprint with the soft PDMS and PDMS–HSQ mold, respectively (scale: 2 μm).

oxygen plasma [32] or as a result of PDMS swelling in the solvent of the mold release agent [17]. These cracks increase the overall surface roughness of the imprinted resist. Yet, the purpose of any patterned resist is its use as mask for the pattern transfer in a complementary process such as etching or liftoff. In this sense, the surface roughness of the top of the resist, such as that in Fig. 3(f), has no negative effect on the outcome of the pattern transfer. On the other hand, the surface roughness of the bottom of the imprinted features may have a negative effect on the process outcome because it can be transferred to the underlying substrate by plasma etching and form a micrograss texture [33]. We estimated the surface roughness of the bottom of the nanoimprinted features in the two cases using AFM. We found that the bottom of the features imprinted with a PDMS mold has a root-mean-square roughness (R_{RMS}) of 8.6 nm. This roughness is much higher than that of the PDMS features of the mold with a R_{RMS} of ~ 1.2 nm. Therefore, this roughness was most probably caused by the deformation of PDMS relief features during the imprint. On the contrary, the bottom surface of the features imprinted with the nanocomposite mold is relatively smooth and has a low R_{RMS} value of 2.2 nm. This low roughness is in the same range of that of HSQ features with a R_{RMS} of ~ 1.5 nm. Based on this finding, we conclude that rigid relief features chemically attached to the soft PDMS substrate do not deform during the imprint and therefore ideally transfer the pattern.

The uniqueness of our soft thermal nanoimprint approach is highlighted by the reduction in the feature size. Figure 4 shows arrays of 200-nm features that were thermally nanoimprinted in PBMA with (a) a conventional PDMS mold and (b) our nanocomposite mold. The height of the features in both cases is 150 nm. It is clear that the pattern produced by the conventional PDMS mold is highly distorted. Thus, at this size scale, conventional PDMS molds are completely incompatible with thermal resists. At the same time, the dimensions and shape of the nano-features imprinted with our nanocomposite mold exactly reproduce that of the HSQ relief features, which were imaged using scanning electron microscopy (SEM) immediately after electron-beam lithography (Fig. S4 in the ESM). Therefore, the nanocomposite molds made from PDMS substrates and chemically attached rigid relief features seem to be the ultimate solution for soft thermal nanoimprint lithography with ultra-high patterning resolution.

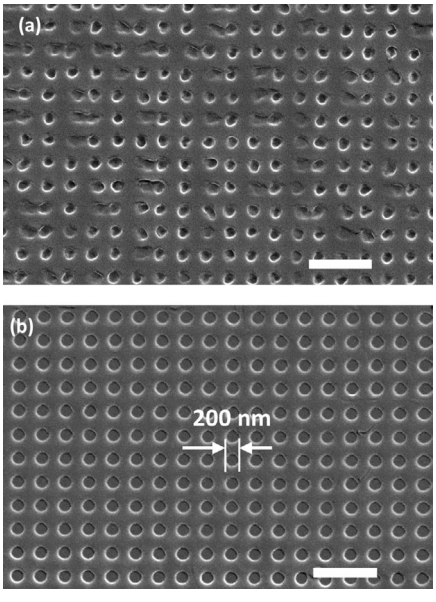

Figure 4 Scanning electron microscopy images of the substrate imprinted with the (a) soft PDMS mold and (b) nanocomposite PDMS–HSQ hybrid mold (scale: 1 μm).

Because our soft thermal nanoimprinting approach is based on a mold composed of an elastomeric substrate and rigid relief features, it uniquely combines the key advantages of both conventional rigid and soft imprints: (i) It has a high resolution comparable to that of nanoimprinting with rigid molds, and (ii) it can easily produce a defect-free conformal contact with an imprinted substrate, even when the substrate is not planar. To demonstrate this unique and innovative combination, we thermally nanoimprinted an ultra-high-resolution pattern on the surface of a lens. For this purpose, we spin-coated and baked a PBMA film on a spherical lens with a diameter of 35 mm and curvature radius of 50 mm. We used a nanocomposite PDMS mold that contained 100-nm HSQ features. We performed the imprint by placing the mold on top of the lens and positioning the lens–mold sandwich between the two membranes in the chuck of a Nanonex NX-B200 nanoimprint tool (Fig. 5(a)). We used the same parameters as described previously for flat substrates for the nanoimprinting process. Notably, we observed no macroscopic distortion or wrinkles on the mold surface during the contact with the used lens (Fig. S5 in the ESM). After the nanoimprinting was completed, we gently separated the mold from the lens surface.

Figure 5(b) shows a SEM image of the imprinted lens surface. Although we used a curved surface for imprinting, the quality of the transferred nanopattern was found to be excellent and comparable to commonly obtained high-resolution thermal nanoimprints on flat surfaces. The SEM images were taken for several locations on the lens, and indicated a negligible (few%) elongation of the array periodicity compared with its nominal value of 300 nm (Fig. 5(b) and Fig. S6 in the ESM). This elongation is the same in both x and y directions. We explain this elongation with isotropic in-plane stretching of the mold that necessarily takes place when it conformally covers the lens surface. Notably, this stretching most likely creates shear forces at the PDMS–HSQ interface during the mold application. These forces, however, do not seem to affect the quality of the imprint or reliability of the mold.

As mentioned above, conventional state-of-the-art soft nanoimprinting is incompatible with thermal

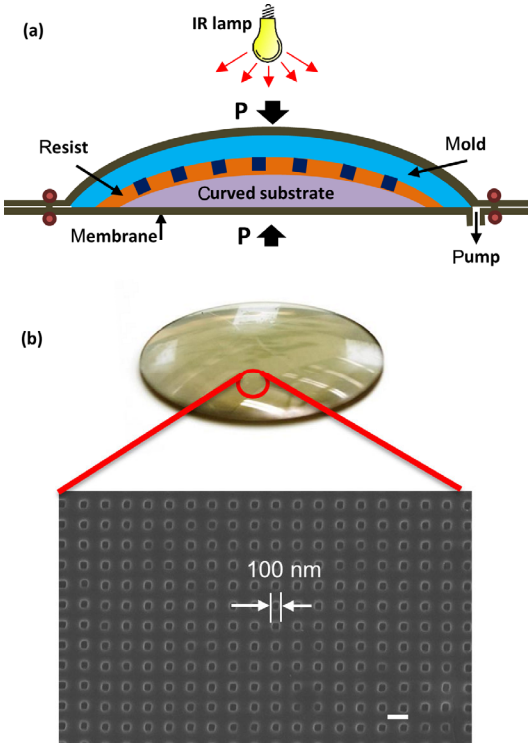

Figure 5 (a) Schematic drawing of imprinting on a curved surface used in this study. (b) Thermal nanoimprint on lens (scale bar on the SEM image = 300 nm).

resists because the polymeric resist and relief features of an elastomeric mold have similar elastic moduli. Thus, elastomeric relief features are not rigid enough to sustain the high capillary forces and pressure applied during the imprint. As a result, these features deform, which causes pattern distortion. Previously reported hybrid molds contained imaging layers made from harder materials, such as hard PDMS [12] and a photocurable polymer [13], whose moduli are 9 and 216 MPa, respectively. The relief features made from these materials were stiff enough to produce quality nanopatterns within low-viscosity UV curable resists. However, we presume that their polymeric imaging features would be substantially softened while heated up to the imprint temperature if such molds were used for thermal nanoimprint. Therefore, they would fail to emboss a highly viscous thermal resist. In contrast to these state-of-the-art hybrid molds, our novel mold contains relief features made from cured HSQ, whose modulus after curing at 330 °C is ~ 10 GPa [34], that is, a few orders of magnitude higher than that of previously reported hybrid molds. Furthermore, due to its highly crosslinked structure,

cured HSQ retains its mechanical properties when heated to 200 °C and above [35]. Therefore, even when heated up to the temperature of thermal imprinting, the HSQ relief features will remain stiff enough to sustain the nanoimprint pressure and penetrate the viscous thermal resist, ensuring a pattern transfer with the highest possible fidelity.

Notably, despite the rigid relief features, our composite mold forms a robust conformal contact with an imprinted surface and minimizes pattern defects, similar to a conventional PDMS mold. Figure S7 (in the ESM) compares a pattern thermally nanoimprinted with a rigid Si-based mold with a similar pattern nanoimprinted with a composite mold. Whereas the surface imprinted with the rigid mold contains clearly visible large-area defects stemming from surface contaminations, the surface imprinted with the composed mold is pristine. A few random contaminants found in the latter imprint form localized pattern defects with sizes not largely exceeding the size of the contaminant itself. As already mentioned, this sustainability in the presence of contaminants is typical for soft elastomeric molds.

State-of-the-art hybrid molds and our nanocomposite PDMS–HSQ mold differ not only with respect to the mechanical properties of the relief features but also with respect to their basic configuration. Specifically, each of the previously reported hybrid molds contains a "stiff" imaging layer. These molds can imprint simple curved surfaces, such as cylindrical shapes, but they cannot imprint surfaces with more complex curvatures such as lenses. Conversely, in our novel mold, the relief features and background surface are made from completely different materials. Whereas the rigidity of the former ensures high pattern resolution and fidelity, the elasticity of the latter enables complete freedom of the mold deformation. Consequently, our mold is compatible with substrates with complex curvatures.

To fabricate our nanocomposite molds, we used electron-beam lithography, which is serial and therefore expensive and time-consuming. Naturally, the demonstrated fabrication route is not as cost-effective as that of conventional PDMS molds. Yet, we believe that other more cost-effective and scalable approaches can be applied to nanocomposite molds. For instance, a silicon oxide film deposited on Au by plasma enhanced chemical vapor deposition (PECVD) or atomic layer deposition (ALD) and then patterned by photolithography could be an alternative for electron-beam-patterned HSQ. Certainly, the size of the rigid features of the mold and its pattern resolution will be limited by the diffraction of light and process conditions used for photolithography in this case. In addition, in this work, we produced molds with a total patterned area of up to a few hundred square micrometers, being limited by the patterning capabilities of electron-beam lithography as a serial process (see Fig. S8 in the ESM for an example of a large-scale pattern transferred to a nanocomposite mold). This area is sufficient for prototype molds. Larger areas can be produced by using parallel patterning methods, such as photolithography or X-ray lithography, or a longer electron-beam exposure. In general, we believe that electron-beam-fabricated nanocomposite molds mostly fit niche applications of nanoimprinting, which require a combination of (i) ultra-high resolution, (ii) thermal resist, and (iii) unconventional or non-planar substrates. To the best of our knowledge, such a combination has not been demonstrated before.

Soft thermal nanoimprinting is a template-assisted method to fabricate micro- and nanostructures. In fact, there are many novel template-free high-resolution nanofabrication methods such as holographic lithography [36–38] and femtosecond laser direct writing [39–41]. However, these methods are based on a focused beam and therefore are unlikely applicable to non-planar substrates. Furthermore, holographic lithography and various self-assembly-based nanofabrication methods, such as nanosphere lithography [42] and block copolymer lithography [43], can produce only periodic structures with a certain geometry. Nanoimprinting, on the contrary, can produce any arbitrary pattern, as demonstrated in this work.

In this work, we used PBMA as a thermal imprint resist. As mentioned above, the choice of PBMA was motivated mainly by its relatively low glass transition temperature of 54 °C, allowing nanoimprinting at 100 °C. In general, the imprinting temperature should be a few tens of degrees above the polymer glass transition to allow viscous flow [44]. The application of commonly used thermal resists such as PMMA with T_g of 105 °C will require an imprint temperature

above 150 ˚C [45]. We speculate that at such a high imprinting temperature, PDMS will become too soft to enable a robust pattern transfer with high fidelity [46]. In addition, imprinting at lower temperatures reduces possible stresses applied onto the mold and the resist forms as the result of the difference in their thermal expansion coefficients [47]. We believe that in addition to PBMA, many other polymers with T_g < 100 ˚C may be used for soft thermal imprinting such as poly(3-hexylthiophen) [48], polyethylene terephthalate [49], polyvinyl butyral (PVB) [50], and polyethyleneimine (PEI) [51].

In summary, we introduce a novel nanoimprinting approach that enables the nanopatterning of thermoplastic resists with soft elastomeric molds. This combination of "soft" and "thermal" is unprecedented for nanoimprint lithography and became possible due to the unique structure of the mold that combines an elastomeric substrate with chemically attached rigid relief features. Such a mold can be fabricated in a robust process based on the transfer of features from a sacrificial substrate to a PDMS membrane. We demonstrated high-resolution pattern transfer to thermal resists using flat surfaces and surfaces with a high degree of curvature such as lenses. Our approach paves the way to numerous applications that require thermal processing on substrates with unconventional geometries. These applications include but are not limited to thermal nanopatterning of optical fibers or lenses with antireflective coatings, diffraction gratings and many other functional nanostructures.

Acknowledgements

This work was supported by Adelis Foundation for Renewable Energy (No. 2021611) and Israel Science Foundation (No. 1401/15). Viraj Bhingardive thanks the Negev-Tsin Scholarship for its support.

Electronic Supplementary Material: Supplementary material (experimental details, supplementary figures) is available in the online version of this article at https://doi.org/10.1007/s12274-017-1900-0.

References

[1] Xia, Y. N.; Whitesides, G. M. Soft lithography. *Annu. Rev. Mater. Sci.* **1998**, *28*, 153–184.

[2] Qin, D.; Xia, Y. N.; Whitesides, G. M. Soft lithography for micro- and nanoscale patterning. *Nat. Protoc.* **2010**, *5*, 491–502.

[3] Guo, L. J. Nanoimprint lithography: Methods and material requirements. *Adv. Mater.* **2007**, *19*, 495–513.

[4] Legrand, D. G.; Gaines, G. L., Jr. The molecular weight dependence of polymer surface tension. *J. Colloid Interface Sci.* **1969**, *31*, 162–167.

[5] Jung, G. Y.; Li, Z. Y.; Wu, W.; Chen, Y.; Olynick, D. L.; Wang, S. Y.; Tong, W. M.; Williams, R. S. Vapor-phase self-assembled monolayer for improved mold release in nanoimprint lithography. *Langmuir* **2005**, *21*, 1158–1161.

[6] Moran, I. W.; Briseno, A. L.; Loser, S.; Carter, K. R. Device fabrication by easy soft imprint nano-lithography. *Chem. Mater.* **2008**, *20*, 4595–4601.

[7] Fan, Z. Y.; Razavi, H.; Do, J.-W.; Moriwaki, A.; Ergen, O.; Chueh, J. L.; Leu, P. W.; Ho, J. C.; Takahashi, T.; Reichertz, L. A. et al. Three-dimensional nanopillar-array photovoltaics on low-cost and flexible substrates. *Nat. Mater.* **2009**, *8*, 648–653.

[8] Chen, J. W.; Gu, C. L.; Lin, H.; Chen, S.-C. Soft mold-based hot embossing process for precision imprinting of optical components on non-planar surfaces. *Opt. Express* **2015**, *23*, 20977–20985.

[9] Delamarche, E.; Schmid, H.; Michel, B.; Biebuyck, H. Stability of molded polydimethylsiloxane microstructures. *Adv. Mater.* **1997**, *9*, 741–746.

[10] Hua, F.; Sun, Y. G.; Gaur, A.; Meitl, M. A.; Bilhaut, L.; Rotkina, L.; Wang, J. F.; Geil, P.; Shim, M.; Rogers, J. A. et al. Polymer imprint lithography with molecular-scale resolution. *Nano Lett.* **2004**, *4*, 2467–2471.

[11] Schmid, H.; Michel, B. Siloxane polymers for high-resolution, high-accuracy soft lithography. *Macromolecules* **2000**, *33*, 3042–3049.

[12] Odom, T. W.; Love, J. C.; Wolfe, D. B.; Paul, K. E.; Whitesides, G. M. Improved pattern transfer in soft lithography using composite stamps. *Langmuir* **2002**, *18*, 5314–5320.

[13] Li, Z. W.; Gu, Y. N.; Wangs, L.; Ge, H. X.; Wu, W.; Xia, Q. F.; Yuan, C. S.; Chen, Y. F.; Cui, B.; Williams, R. S. Hybrid nanoimprint-soft lithography with sub-15 nm resolution. *Nano Lett.* **2009**, *9*, 2306–2310.

[14] Richeton, J.; Ahzi, S.; Vecchio, K. S. S.; Jiang, F. C.; Adharapurapu, R. R. Influence of temperature and strain rate on the mechanical behavior of three amorphous polymers: Characterization and modeling of the compressive yield stress. *Int. J. Solids Struct.* **2006**, *43*, 2318–2335.

[15] Wang, Z. X.; Volinsky, A. A.; Gallant, N. D. Crosslinking effect on polydimethylsiloxane elastic modulus measured by custom-built compression instrument. *J. Appl. Polymer Sci.* **2014**, *131*, 41050.

[16] Chuah, Y. J.; Koh, Y. T.; Lim, K.; Menon, N. V.; Wu, Y. N.; Kang, Y. J. Simple surface engineering of polydimethylsiloxane

with polydopamine for stabilized mesenchymal stem cell adhesion and multipotency. *Sci. Rep.* **2015**, *5*, 18162.

[17] Lee, J. N.; Park, C.; Whitesides, G. M. Solvent compatibility of poly(dimethylsiloxane)-based microfluidic devices. *Anal. Chem.* **2003**, *75*, 6544–6554.

[18] Menahem, L.; Schvartzman, M. Soft nanoimprint mold with rigid relief features for improved pattern transfer. *J. Vac. Sci. Technol. B* **2017**, *35*, 010602.

[19] Maex, K.; Baklanov, M. R.; Shamiryan, D.; Lacopi, F.; Brongersma, S. H.; Yanovitskaya, Z. S. Low dielectric constant materials for microelectronics. *J. Appl. Phys.* **2003**, *93*, 8793–8841.

[20] Yamazaki, K.; Namatsu, H. 5-nm-order electron-beam lithography for nanodevice fabrication. *Jpn. J. Appl. Phys.* **2004**, *43*, 3767–3771.

[21] Bhattacharya, S.; Datta, A.; Berg, J. M.; Gangopadhyay, S. Studies on surface wettability of poly(dimethyl) siloxane (PDMS) and glass under oxygen-plasma treatment and correlation with bond strength. *J. Microelectromech. Syst.* **2005**, *14*, 590–597.

[22] McDonald, J. C.; Duffy, D. C.; Anderson, J. R.; Chiu, D. T.; Wu, H. K.; Schueller, O. J. A.; Whitesides, G. M. Fabrication of microfluidic systems in poly(dimethylsiloxane). *Electrophoresis* **2000**, *21*, 27–40.

[23] Schvartzman, M.; Palma, M.; Sable, J.; Abramson, J.; Hu, X.; Sheetz, M. P.; Wind, S. J. Nanolithographic control of the spatial organization of cellular adhesion receptors at the single-molecule level. *Nano Lett.* **2011**, *11*, 1306–1312.

[24] Schuster, B.-E.; Haug, A.; Häffner, M.; Blideran, M. M.; Fleischer, M.; Peisert, H.; Kern, D. P.; Chassé, T. Characterization of the morphology and composition of commercial negative resists used for lithographic processes. *Anal. Bioanal. Chem.* **2009**, *393*, 1899–1905.

[25] Yuan, Q. H..; Yin, G. Q.; Ning, Z. Y. Effect of oxygen plasma on low dielectric constant HSQ (Hydrogensilsesquioxane) films. *Plasma Sci. Technol.* **2013**, *15*, 86–88.

[26] Kawamori, M.; Nakamatsu, K.; Haruyama, Y.; Matsui, S. Effect of oxygen plasma irradiation on hydrogen silsesquioxane nanopatterns replicated by room-temperature nanoimprinting. *Jpn. J App. Phys.* **2006**, *45*, 8994–8996.

[27] Cai, H. G.; Wind, S. J. Improved glass surface passivation for single-molecule nanoarrays. *Langmuir* **2016**, *32*, 10034–10041.

[28] Yang, K.-Y.; Yoon, K.-M.; Kim, J.-W.; Lee, J.-H.; Lee, H. Low temperature fabrication of residue-free polymer patterns on flexible polymer substrate. *Jpn. J. Appl. Phys.* **2009**, *48*, 095003.

[29] Liu, M.; Sun, J. R.; Chen, Q. F. Influences of heating temperature on mechanical properties of polydimethylsiloxane. *Sens. Actuators A: Phys.* **2009**, *151*, 42–45.

[30] Lötters, J. C.; Olthuis, W.; Veltink, P. H.; Bergveld, P. The mechanical properties of the rubber elastic polymer polydimethylsiloxane for sensor applications. *J. Micromech. Microeng.* **1997**, *7*, 145–147.

[31] Gates, B. D.; Whitesides, G. M. Replication of vertical features smaller than 2 nm by soft lithography. *J. Am. Chem. Soc.* **2003**, *125*, 14986–14987.

[32] Hillborg, H.; Ankner, J. F.; Gedde, U. W.; Smith, G. D.; Yasuda, H. K.; Wikström, K. Crosslinked polydimethylsiloxane exposed to oxygen plasma studied by neutron reflectometry and other surface specific techniques. *Polymer* **2000**, *41*, 6851–6863.

[33] Gogolides, E.; Constantoudis, V.; Kokkoris, G.; Kontziampasis, D.; Tsougeni, K.; Boulousis, G.; Vlachopoulou, M.; Tserepi, A. Controlling roughness: From etching to nanotexturing and plasma-directed organization on organic and inorganic materials. *J. Phys. D: Appl. Phys.* **2011**, *44*, 174021.

[34] Liou, H.-C.; Pretzer, J. Effect of curing temperature on the mechanical properties of hydrogen silsesquioxane thin films. *Thin Solid Films* **1998**, *335*, 186–191.

[35] Chung, S. W.; Shin, J. H.; Park, N. H.; Park, J. W. Dielectric properties of hydrogen silsesquioxane films degraded by heat and plasma treatment. *Jpn. J. Appl. Phys.* **1999**, *38*, 5214–5219.

[36] Oh, Y.; Lim, J. W.; Kim, J. G.; Wang, H.; Kang, B.-H.; Park, Y. W.; Kim, H.; Jang, Y. J.; Kim, J.; Kim, D. H. et al. Plasmonic periodic nanodot arrays via laser interference lithography for organic photovoltaic cells with > 10% efficiency. *ACS Nano* **2016**, *10*, 10143–10151.

[37] Bi, Y.-G.; Feng, J.; Li, Y.-F.; Zhang, X.-L.; Liu, Y.-F.; Jin, Y.; Sun, H.-B. Broadband light extraction from white organic light-emitting devices by employing corrugated metallic electrodes with dual periodicity. *Adv. Mater.* **2013**, *25*, 6969–6974.

[38] Jin, Y.; Feng, J.; Zhang, X.-L.; Bi, Y.-G.; Bai. Y.; Chen, L.; Lan, T.; Liu, Y.-F.; Chen, Q.-D.; Sun, H.-B. Solving efficiency-stability tradeoff in top-emitting organic light-emitting devices by employing periodically corrugated metallic cathode. *Adv. Mater.* **2012**, *24*, 1187–1191.

[39] Bi, Y.-G.; Feng, J.; Li, Y.-F.; Zhang, Y.-L.; Liu, Y.-S.; Chen, L.; Liu, Y.-F.; Guo, L.; Wei, S.; Sun, H.-B. Arbitrary shape designable microscale organic light-emitting devices by using femtosecond laser reduced graphene oxide as a patterned electrode. *ACS Photonics* **2014**, *1*, 690–695.

[40] Fujita, Y.; Aubert, R.; Walke, P.; Yuan, H.; Kenens, B.; Inose, T.; Steuwe, C.; Toyouchi, S.; Fortuni, B.; Chamtouri, M. et al. Highly controllable direct femtosecond laser writing of gold nanostructures on titanium dioxide surfaces. *Nanoscale* **2017**, *9*, 13025–13033.

[41] Xiong, W.; Zhou, Y. S.; He, X. N.; Gao, Y.; Mahjouri-Samani, M.; Jiang, L.; Baldacchini, T.; Lu, Y. F. Simultaneous additive and subtractive three-dimensional nanofabrication using integrated two-photon polymerization and multiphoton ablation. *Light Sci. Appl.* **2012**, *1*, e6.

[42] Haynes, C. L.; Van Duyne, R. P. Nanosphere lithography: A versatile nanofabrication tool for studies of size-dependent nanoparticle optics. *J. Phys. Chem. B* **2001**, *105*, 5599–5611.

[43] Bates, C. M.; Maher, M. J.; Janes, D. W.; Ellison, C. J.; Willson, C. G. Block copolymer lithography. *Macromolecules* **2014**, *47*, 2–12.

[44] Guo, L. J. Recent progress in nanoimprint technology and its applications. *J. Phys. D: Appl. Phys.* **2004**, *37*, R123–R141.

[45] Chou, S. Y.; Krauss, P. R.; Renstrom, P. J. Imprint lithography with 25-nanometer resolution. *Science* **1996**, *272*, 85–87.

[46] Johnston, I. D.; McCluskey, D. K.; Tan, C. K. L.; Tracey, M. C. Mechanical characterization of bulk Sylgard 184 for microfluidics and microengineering. *J. Micromech. Microeng.* **2014**, *24*, 035017.

[47] Kim, B.; Park, M.; Kim, Y. S.; Jeong, U. Thermal expansion and contraction of an elastomer stamp causes position-dependent polymer patterns in capillary force lithography. *ACS Appl. Mater. Interfaces* **2011**, *3*, 4695–4702.

[48] Cheyns, D.; Vasseur, K.; Rolin, C.; Genoe, J.; Poortmans, J.; Heremans, P. Nanoimprinted semiconducting polymer films with 50 nm features and their application to organic heterojunction solar cells. *Nanotechnology* **2008**, *19*, 424016.

[49] Cecchini, M.; Signori, F.; Pingue, P.; Bronco, S.; Ciardelli, F.; Beltram, F. High-resolution poly(ethylene terephthalate) (PET) hot embossing at low temperature: Thermal, mechanical, and optical analysis of nanopatterned films. *Langmuir* **2008**, *24*, 12581–12586.

[50] Juang, Y.-J.; Lee, L. J.; Koelling, K. W. Hot embossing in microfabrication. Part I: Experimental. *Polymer Eng. Sci.* **2002**, *42*, 539–550.

[51] Subramani, C.; Ofir, Y.; Patra, D.; Jordan, B. J.; Moran, I. W.; Park, M.-H.; Carter, K. R.; Rotello, V. M. Nanoimprinted polyethyleneimine: A multimodal template for nanoparticle assembly and immobilization. *Adv. Funct. Mater.* **2009**, *19*, 2937–2942.